

Research Article

Diffusivity-limited q-space trajectory imaging

Deneb Boito ^{a, b, *}, Magnus Herberthson ^c, Tom Dela Haije ^d, Ida Blystad ^{b, e},
Evren Özarslan ^{a, b, **}

^a Department of Biomedical Engineering, Campus US, Linköping University, Linköping, SE-581 83, Sweden

^b Center for Medical Image Science and Visualization, Linköping University, Linköping, SE-581 83, Sweden

^c Department of Mathematics, Linköping University, Linköping, SE-581 83, Sweden

^d Department of Computer Science, University of Copenhagen, Copenhagen, DK-2300, Denmark

^e Department of Radiology in Linköping and Department of Health, Medicine and Caring Sciences, Linköping University, Linköping, SE-581 83, Sweden

ARTICLE INFO

Article history:

Received 28 September 2022

Received in revised form 13 December 2022

Accepted 25 December 2022

Available online 6 January 2023

Keywords:

Diffusion

Diffusion MRI

q-space trajectory imaging

QTI

Microstructure

Microscopic anisotropy

QTI+

Constrained

ABSTRACT

Q-space trajectory imaging (QTI) allows non-invasive estimation of microstructural features of heterogeneous porous media via diffusion magnetic resonance imaging performed with generalised gradient waveforms. A recently proposed constrained estimation framework, called QTI+, improved QTI's resilience to noise and data sparsity, thus increasing the reliability of the method by enforcing relevant positivity constraints. In this work we consider expanding the set of constraints to be applied during the fitting of the QTI model. We show that the additional conditions, which introduce an upper bound on the diffusivity values, further improve the retrieved parameters on a publicly available human brain dataset as well as on data acquired from healthy volunteers using a scanner-ready protocol.

© 2023 The Authors. Publishing services by Elsevier B.V. on behalf of KeAi Communications Co. Ltd. This is an open access article under the CC BY-NC-ND license (<http://creativecommons.org/licenses/by-nc-nd/4.0/>).

1. Introduction

Diffusion magnetic resonance imaging (dMRI) is an imaging technique possessing exquisite inherent sensitivity to the random motion of water molecules, which can be exploited to determine local features of complex porous media. The random motion can be encoded into the MR signal by means of time-varying magnetic field gradients, and interpreted using (bio) physical models or signal representations. In Q-space trajectory imaging (QTI) [1], the medium is imaged as being composed of several non-exchanging gaussian compartments, each represented by a diffusion tensor [2]. As such, each voxel is represented using a diffusion tensor distribution (DTD) [3]. At low diffusion sensitivities achieved with general gradient waveforms, QTI gives access to the first statistical moments of the DTD via the cumulant expansion. These are quantified in a 3×3 symmetric positive semidefinite matrix denoting the average diffusion tensor, and a fourth order object denoting the covariance of the diffusion tensors — the two quantities that define a tensor-variate normal distribution [4]. From these two, it is possible to compute a series of metrics which are sensitive to different microstructural features of porous structures. Akin

* Corresponding author. Department of Biomedical Engineering, Campus US, Linköping University, Linköping, SE-581 83, Sweden.

** Corresponding author. Department of Biomedical Engineering, Campus US, Linköping University, Linköping, SE-581 83, Sweden.

E-mail addresses: deneb.boito@liu.se (D. Boito), evren.ozarslan@liu.se (E. Özarslan).

Peer review under responsibility of Innovation Academy for Precision Measurement Science and Technology (APM), CAS.

to what is done for characterizing size distributions [5], the goal in QTI is to estimate the statistical moments of the DTD from the collected data, and use these to interpret structural properties of complex media.

Herberthson et al. recently introduced a framework called QTI+ [6], which improved QTI's robustness to noise thus increasing its reliability. This was accomplished by imposing relevant positivity constraints as was done for other diffusion MR models [7]. It was shown that by performing the constrained estimation, it was possible to obtain more accurate parameter estimates which seemed to promote smoothness in the derived maps, despite each voxel being fitted independently [6]. Moreover, it was found that the constrained fit lowered the demand on the number of diffusion measurements to be acquired and considered for the estimation [8]. In addition to these encouraging findings, we encountered unrealistically high values of some of the scalar measures particularly in voxels with a large cerebrospinal fluid (CSF) content. To address this issue, in this work we formulate and apply complementary constraints which prohibit water diffusivity to exceed its theoretical physical value. Other works also considered imposing upper bounds while estimating metrics in other diffusion models, such as diffusion kurtosis imaging [9,10]. We thus incorporate the new constraints into the QTI+ framework, determine the extent of the violations of such conditions, and observe how imposing them influences the QTI metrics on human brain data obtained from a GE scanner.

2. Methods

2.1. Theory

2.1.1. Notation

The notation in this work is kept consistent with the one used in Ref. [6]. In short, italic characters are reserved for scalar quantities, boldface characters are used for matrices and second order tensors, and blackboard bold (double struck) characters denote fourth-order tensors. By choosing a basis in the 6-dimensional space of symmetric 3×3 matrices, all their mutual tensor products give 6×6 elements of the same type as the fourth order tensors occurring here. Hence these fourth order tensors can be represented as 6×6 matrices, and the tensor symmetries also imply that these 6×6 matrices are symmetric.

For the indexing, when expressed through Latin letters i, j, k , and l , they range from 1 to 3, while when expressed through the early Greek letters α, β , and γ , they range from 1 to 6. As an example, \mathbb{A}_{ijkl} and $\mathbf{A}_{\alpha\beta}$ are the fourth order and second order representations of the same tensor. When used with double struck and boldface characters, the indices do not refer to a particular component of the tensor but rather to the order of the elements. As explained in Ref. [6], the components of a tensor are addressed using ordinary capital letters, e.g., A_{ij} . The matrix products are expressed using the Einstein summation convention.

2.1.2. QTI

QTI [1] is a framework utilizing diffusion measurements with time varying magnetic field gradients and a diffusion tensor distribution [3] model, with stochastic variable \mathbf{D}_{ij} , for the medium microstructure. The DTD model assumes Gaussian diffusion within the subdomains making up the tissue. Consequently, all experimental parameters of each diffusion magnetic resonance experiment are captured by a measurement tensor, which we refer to in the text as \mathbf{B}_{ij} [11]. In the limit of small \mathbf{B}_{ij} , the MR signal in QTI is interpreted through the first two statistical cumulants of the DTD, namely the mean $\hat{\mathbf{D}}_{ij} = \langle \mathbf{D}_{ij} \rangle$ and fourth order covariance tensor $\mathbb{C}_{ijkl} = \langle (\mathbf{D}_{ij} - \hat{\mathbf{D}}_{ij}) \otimes (\mathbf{D}_{kl} - \hat{\mathbf{D}}_{kl}) \rangle$. The MR signal, via cumulant expansion, can thus be written as [1]:

$$S(\mathbf{B}_{ij}) = S_0 \exp\left(-B_{ij}\hat{\mathbf{D}}_{ij} + \frac{1}{2}B_{ij}B_{kl}C_{ijkl}\right). \quad (1)$$

Given a family of measurements \mathbf{B}_{ij} , the parameters S_0 , $\hat{\mathbf{D}}_{ij}$, and \mathbb{C}_{ijkl} can be estimated by solving the following problem:

$$\underset{S_0, \hat{\mathbf{D}}_{ij}, \mathbb{C}_{ijkl}}{\operatorname{argmin}} \sum_{n=1}^N \left| S_n - S_0 e^{-B_{ij}^{(n)} \hat{\mathbf{D}}_{ij} + \frac{1}{2} B_{ij}^{(n)} B_{kl}^{(n)} C_{ijkl}} \right|^2 \quad (2)$$

which upon linearization by taking the logarithm becomes the weighted linear least squares problem:

$$\underset{S_0, \hat{\mathbf{D}}_{ij}, \mathbb{C}_{ijkl}}{\operatorname{argmin}} \sum_{n=1}^N S_n^2 \left| \ln(S_n) - \ln(S_0) + B_{ij}^{(n)} \hat{\mathbf{D}}_{ij} - \frac{1}{2} B_{ij}^{(n)} B_{kl}^{(n)} C_{ijkl} \right|^2 \quad (3)$$

where the heteroskedasticity introduced by the logarithmic operation is accounted for by the factor S_n^2 . The problems defined in equations (2) and (3) can be solved by traditional non-linear and (weighted) linear least squares routines, respectively.

2.1.3. QTI+

In QTI+, the problems defined in equations (2) and (3) are solved while necessary positivity conditions are applied on the tensors to be estimated using non-linear and semidefinite programming (SDP) routines. The applied conditions were named

‘(d)’, ‘(c)’, and ‘(m)’, with the letters indicating which tensor the condition is imposed on. Here, ≥ 0 stands for positive semi-definite in the sense that all eigenvalues are non-negative:

(d) $\widehat{\mathbf{D}}_{ij} \geq 0$,

(c) $\mathbf{C}_{\alpha\beta} \geq 0$, and

(m) for all \mathbf{v}_i and \mathbf{u}_i , $M_{ijkl} v_i v_j u_k u_l \geq 0$

where M_{ijkl} are the elements of the fourth order tensor $\mathbb{M}_{ijkl} = \mathbb{C}_{ijkl} + \widehat{\mathbf{D}}_{ij} \otimes \widehat{\mathbf{D}}_{kl}$.

2.1.4. Diffusivity-limiting conditions

In this section, we describe additional conditions that could be imposed. In particular, the earlier conditions are expanded based on the observation that the maximum values of the diffusivities must be bounded from above. This maximum allowed value could be specified to be the bulk diffusivity D_0 for free diffusion occurring at a certain temperature. Mathematically, this translates into saying that $\widehat{\mathbf{D}}_{ij} - D_0 \mathbf{I}_{ij}$ must be negative semidefinite for some bulk diffusivity D_0 . We refer to this condition as (d_{SL}) , where SL stands for ‘speed limit’:

$(d_{SL}) \quad \widehat{\mathbf{D}}_{ij} - D_0 \mathbf{I}_{ij} \leq 0$

The same reasoning applied to the covariance tensor \mathbb{C}_{ijkl} results in several constraints. Below, the components C_{ijkl} are expressed with respect to an orthonormal basis, and the coefficients $C_{\alpha\beta}$ with respect to a basis which is discussed in the appendix:

$(c1_{SL}) \quad -D_0^2/4 \leq C_{\alpha\beta} \leq D_0^2/4$ and $0 \leq C_{\alpha\alpha} \leq D_0^2/4$, if $1 \leq \alpha, \beta \leq 3$

$(c2_{SL}) \quad 0 \leq \lambda_i \leq \frac{3}{4} D_0^2, i = 1, 2, 3, 4, 5, 6$, where λ_i are the eigenvalues of $\mathbf{C}_{\alpha\beta}$

$(\Gamma_{SL}^+) \quad \left(C_{ijkl} + \frac{D_0^2}{4} I_{ij} I_{kl} \right) u_i u_j u_k u_l \geq 0$

$(\Gamma_{SL}^-) \quad \left(C_{ijkl} - \frac{D_0^2}{4} I_{ij} I_{kl} \right) u_i u_j u_k u_l \leq 0$

When applied on the tensor \mathbb{M}_{ijkl} , this constraint results in the condition

$(m_{SL}) \quad \left(M_{ijkl} - D_0^2 I_{ij} I_{kl} \right) u_i u_j u_k u_l \leq 0$

To apply these constraints, one is forced to determine the appropriate D_0 to be used as maximum allowed diffusivity. This value is mostly depending on the water temperature at the moment the experiment is performed. As there is no simple way of measuring this, the chosen threshold will most likely be an approximation of what the correct one should be. The discussion around possible choices of this value for human brain dMRI acquisition is found in later sections.

2.2. QTI±

The conditions derived in the previous sections can be applied alongside those enforced in QTI+ using semidefinite programming. Fig. 1 shows how both the positivity and diffusivity-limiting conditions are enforced in the newly created QTI± framework. In the nomenclature, the ‘-’ sign refers to the diffusivity-limiting conditions, while the ‘+’ sign refers to the non-negativity constraints.

In the $SDP(dc_{\pm})$ step, conditions (d), (c), (d_{SL}) , $(c1_{SL})$, $(c2_{SL})$, and (Γ_{SL}^-) are enforced. Note that condition (Γ_{SL}^+) does not need to be applied, as it is already implied by condition (c). The results obtained in this step can then be checked to verify whether they satisfy conditions (m) and (m_{SL}) . As it was explained in QTI+ [6], these conditions can be checked with a semidefinite programming approach. If both are satisfied, then the results obtained in $SDP(dc_{\pm})$ are the final result. If instead either “m” condition is violated, $SDP(dcm_{\pm})$, which imposes conditions (c), (m), $(c1_{SL})$, (Γ_{SL}^-) and (m_{SL}) , is performed. In this step, the estimated values obtained for \mathbf{D}_{ij} in $SDP(dc_{\pm})$, which are already guaranteed to satisfy conditions (d) and (d_{SL}) , are fixed, so that \mathbb{M}_{ijkl} is linear in the variables to be estimated.

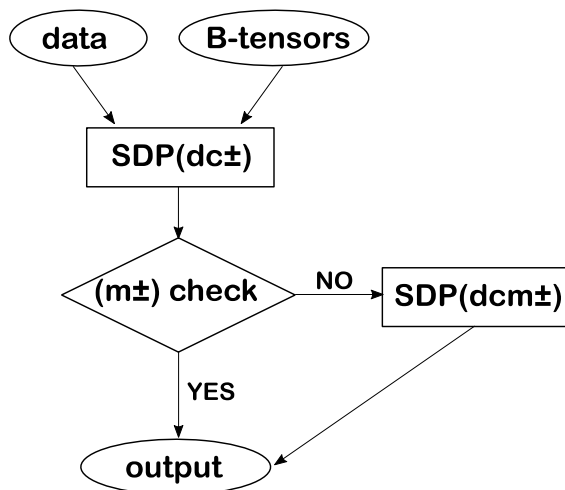


Fig. 1. QTI \pm framework. First, the data and b-tensors are input to the SDP(dc \pm) method. The produced estimates are checked for violations of both conditions (m) and (m_{SL}). If both are satisfied, the obtained parameters constitute the output of the framework. Otherwise, the estimates produced in SDP(dc \pm) are used as starting point in SDP(dcm \pm), which then produces the final estimates for the model parameters.

Note that while the framework depicted in Fig. 1 is what we find to provide the best solutions, it is not compulsory to execute all of its steps. For example, one option could be to take the output of SDP(dc \pm) as the final result. Another option is to skip the check on conditions (m) and (m_{SL}), and directly execute SDP(dcm \pm) after SDP(dc \pm). The results presented in later sections and the run times reported in Table 1 should provide the necessary information for the users to make an informed decision on which option to choose.

2.3. Implementation

The functions performing the constrained fit with both positivity and diffusivity-limiting conditions were implemented in Matlab as an extension to the *qtiplus* software available at <https://github.com/DenebBoito/qtiplus> and described in Ref. [12]. Two SDP optimizers, namely SDPT3 [13] and MOSEK (MOSEK ApS, Denmark), interfaced via CVX [14,15], were interchangeably used to fit the model to the data, and to check the violations of the (m) and (m_{SL}) conditions.

2.4. Violations of the conditions

A publicly available and thoroughly sampled human brain dataset, described in Ref. [16] and available at https://github.com/filip-szczepankiewicz/Szczepankiewicz_DIB_2019, was used to investigate where the diffusivity-limiting conditions are violated on model parameter estimates produced with the QTI+ (SDP(dcm+) method) framework. To simulate shorter acquisitions, this dataset was downsampled as described in Ref. [6], to produce datasets comprising, respectively, 217, 81, 56, and 39 diffusion measurements. We refer to these datasets as, respectively, p217, p81, p56, and p39. These datasets are available at https://github.com/filip-szczepankiewicz/Szczepankiewicz_DIB_2019/tree/master/DATA/brain/NIL_Boito_SubSamples.

First, to verify the violations' dependence on the set maximum allowed bulk diffusivity D_0 , the diffusivity-limiting conditions were checked on model parameter estimates produced on the p81 datasets for 5 different D_0 values. These D_0 values were derived from the work of Holz et al. [17], for water temperatures in the range [36.5°C – 39.5°C].

Secondly, to assess whether the violations exhibit some dependence on the amount of available data, the conditions were checked on the p217, p81, p56, and p39 for the same maximum allowed bulk diffusivity $D_0 = 3.0750 \mu\text{m}^2/\text{ms}$.

Table 1
Run times for different estimation methods in the QTI+ and QTI \pm frameworks. The times were clocked while fitting one of the collected datasets (≈ 60000 voxels).

Method	Run time
SDP(dc+)	7 min
SDP(dc±)	22 min
SDP(dcm+)	9 min
SDP(dcm±)	50 min
m-check + SDP(dcm+)	7 min
m-check + SDP(dcm±)	48 min

2.5. Experimental data

Data from 8 healthy volunteers were collected with ethical approval from the Swedish Ethical Review Authority (Dnr 2019–06123) on a clinical GE Signa Architect 3T MR scanner using a q-space trajectory imaging diffusion protocol. The imaging parameters were: TE = 122 ms, TR = 3289 ms, field-of-view = $240 \times 240 \times 304 \text{ mm}^3$, matrix size = $80 \times 80 \times 39$, voxel size = $3 \times 3 \times 4 \text{ mm}^3$ with 4 mm spacing between slices. The QTI protocol consisted of 122 diffusion measurements organized as follows:

LTE: 6, 6, 16, and 30 directions at, respectively, $b = [0.1, 0.7, 1.4, 2.0] \mu\text{m}^2/\text{ms}$

PTE: 6, 10, and 15 directions at, respectively, $b = [0.1, 1.0, 2.0] \mu\text{m}^2/\text{ms}$

STE: 6, 6, 10, and 10 directions at, respectively, $b = [0.1, 0.7, 1.4, 2.0] \mu\text{m}^2/\text{ms}$

where LTE stands for linear tensor encoding, PTE for planar tensor encoding, STE for spherical tensor encoding, and b is the trace of the measurement tensor \mathbf{B}_{ij} . Prior to model fitting, the data were preprocessed for motion and eddy current corrections using the *eddy* tool from FSL [18] interfaced via *MRtrix3* [19] with default parameters.

3. Results

3.1. Violations of the conditions

Fig. 2 shows where the violations of conditions (d_{SL}) , $(c1_{SL})$, $(c2_{SL})$, (Γ_{SL}^-) , and (m_{SL}) occur. The voxels are color-coded based on which condition is violated in them: blue for the condition on \mathbf{D}_{ij} ((d_{SL})), red for for the conditions on \mathbf{C}_{ijkl} ($(c1_{SL})$, $(c2_{SL})$ and (Γ_{SL}^-)), and green for the condition on \mathbb{M}_{ijkl} ((m_{SL})). The (dcm_{SL}) column shows the voxels in which at least one of the diffusivity limiting conditions is violated; the color there is based on an RGB colormap resulting from the sum of the first 5 columns.

The maps in panel a), obtained on the p81 protocol, highlight how the violations are independent of the maximum allowed diffusivity, for the considered values. The maps in panel b) show that the violations are consistent — in terms of occurring in regions where there is abundance of free water — for model parameters estimated from datasets comprising different numbers of diffusion measurements. From both panels, it is evident that the conditions on the maximum allowed diffusivity are violated almost exclusively in tissues containing large fractions of cerebrospinal fluid (CSF).

3.2. Imposing the conditions

Fig. 3 shows on the left the violations of the diffusivity limiting conditions on fits produced with the unconstrained routine (as implemented in <https://github.com/markus-nilsson/md-dmri>), QTI+, SDP(dc_{\pm}), and SDP(dcm_{\pm}). The resulting QTI stains (Mean Diffusivity (MD), Fractional Anisotropy (FA), microscopic Fractional Anisotropy (μ FA), Size Variance (C_{MD}), and

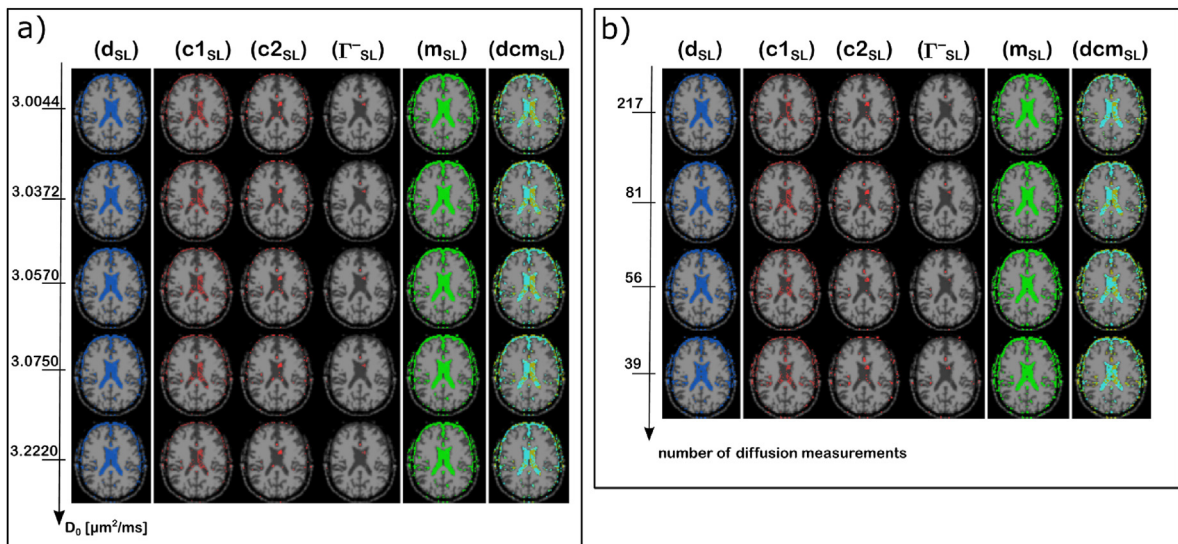


Fig. 2. Violations of the conditions for different choices of D_0 and protocol p81 (panel a), and the considered protocols and maximum allowed diffusivity $D_0 = 3.0750 \mu\text{m}^2/\text{ms}$ (panel b). Colors are used to indicate which of the conditions is violated in each voxel: blue for (d_{SL}) , red for $(c1_{SL})$, $(c2_{SL})$ and (Γ_{SL}^-) , and green for (m_{SL}) . The (dcm_{SL}) column shows all the voxels in which at least one of the conditions is violated as a sum of the first 5 columns RGB values. The model parameters on which the conditions are checked are produced with QTI+ (SDP(dcm_{+})). Both panels highlight how, within the range of considered scenarios, the violations are largely independent of the set maximum allowed diffusivity, and number of diffusion measurements. Moreover, the violations are almost entirely limited to tissues containing a significant amount of CSF.

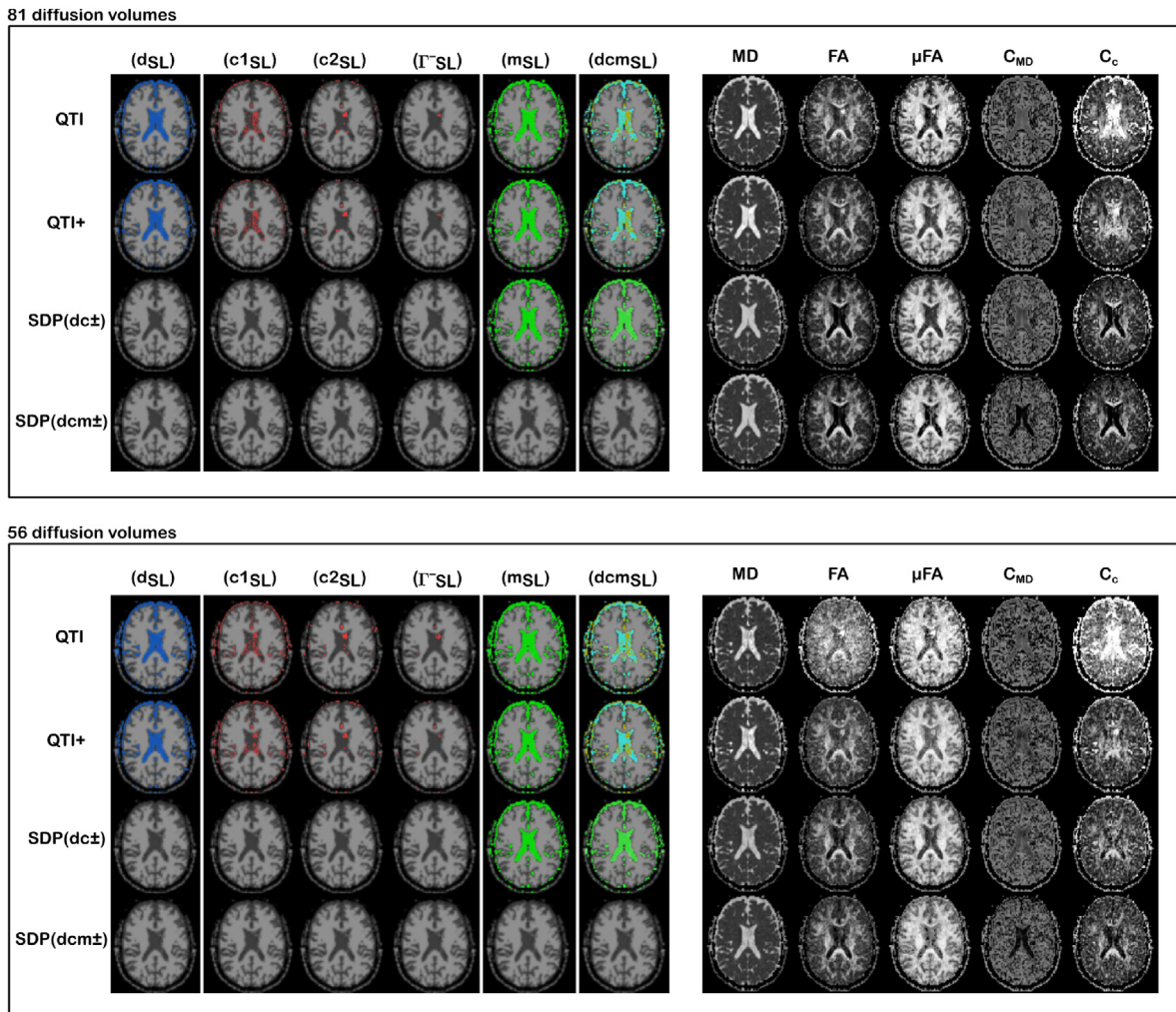


Fig. 3. Violations of the conditions (left) and scalar maps (right) obtained through the p81 (top) and p56 (bottom) protocols. The maximum allowed diffusivity was set to $D_0 = 3.0750 \mu\text{m}^2/\text{ms}$.

Orientation Coherence (C_c) are shown on the right. The model fitting was performed on the p81 (top panel) and p56 (bottom panel) protocols. The violation maps for $\text{SDP}(\text{dc}\pm)$ and $\text{SDP}(\text{dcm}\pm)$ highlight how imposing the constraints provides model estimates which satisfy the targeted conditions.

The maps located on the right side in the panels show how the constraints affect the stains derived in the QTI analysis. The conditions imposed in QTI+ provide generally smoother looking maps, while most of the changes introduced by the new constrained framework are most easily observable in the ventricles, where the theoretical value of FA, μFA , C_{MD} , and C_c should be 0, while the value of MD should have an upper limit set by the maximum allowed diffusivity D_0 . The fits produced with $\text{SDP}(\text{dc}\pm)$ already provide an improvement in several maps when compared with those produced in QTI+. In particular, it was possible to remove the flow artefact located in the frontal horn of the left ventricle. The results are further improved when all the diffusivity limiting conditions are applied in $\text{SDP}(\text{dcm}\pm)$. Observe for example how the μFA , C_{MD} , and C_c quantities are further pushed towards their expected value. Note however that on the fit produced on the p56 protocol, μFA seems to erroneously increase in value in the ventricles.

3.3. Experimental data

Fig. 4 shows the scalar maps obtained by fitting the data for two healthy subjects with QTI+, $\text{SDP}(\text{dc}\pm)$ and $\text{SDP}(\text{dcm}\pm)$. Similar to the results obtained on the p56 and p81 datasets, the QTI maps obtained with the extended list of constraints exhibit improved parameter estimation in tissue containing large fractions of CSF. This provides in general better delineation of different anatomical regions, most evidently in C_{MD} and C_c maps.

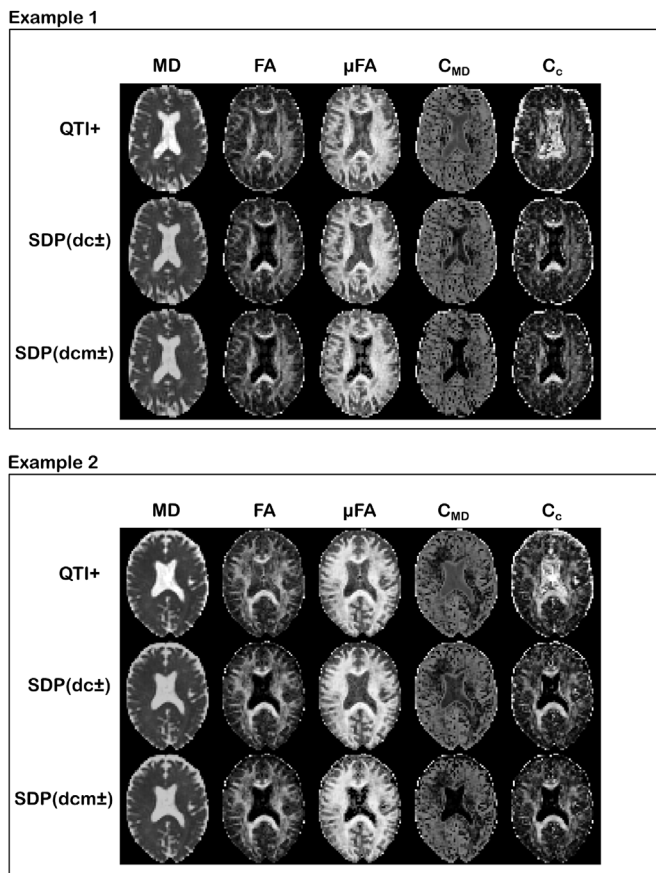


Fig. 4. Example results on two datasets collected on healthy volunteers using a protocol readily available on GE MR scanners. The maximum allowed diffusivity was set to $D_0 = 3.0750 \mu\text{m}^2/\text{ms}$.

3.4. Computational times

In [Table 1](#) we report the run times for the different steps of the QTI_{\pm} framework and representative steps of the QTI_{+} framework, for fittings performed on one of the collected datasets. The run times were recorded on a workstation featuring a 12-core Intel Core i9-7920X CPU. The considered voxels for the fit amounted to ≈ 60000 .

4. Discussion

The results displayed in [Fig. 2](#) highlighted how the violations of the conditions are almost exclusively restricted to areas containing large fractions of CSF. This is perhaps to be expected since in these regions the diffusivity is approximately the same as the speed limit. The results in [Fig. 2](#) panel a) also suggested that when the diffusivity limit is surpassed, it is most likely surpassed by a considerable margin. This consideration could help to relax strict demands on setting an accurate maximum allowed diffusivity to be used for constraining the fit.

Though regions containing *only* free water are typically of little interest for subsequent analysis, we would like to stress that the proposed constraints are relevant for voxels with partial voluming between free water and structures. We show examples of this in [Fig. 5](#). After removing the voxels in which at least one of the eigenvalues of $\hat{\mathbf{D}}$ (estimated with QTI_{+}) exceeds the speed limit, there remain voxels violating condition (m_{SL}). These voxels are most likely located at the interface between white-matter and grey-matter or CSF, i.e., where partial voluming is bound to occur due to the limited achievable spatial resolution. As condition (m_{SL}) is related to the speed limit for each compartment in the voxel's DTD, the violation can be explained by considering that the diffusivity limit is exceeded by the free water fraction in the voxel. In [Fig. 5](#) panel b) we then show how different the QTI stains are in these voxels if estimated with QTI_{+} ($\text{SDP}(\text{dcm}+)$) or QTI_{\pm} ($\text{SDP}(\text{dcm}\pm)$). While, as expected, the metrics computed from $\hat{\mathbf{D}}$ are essentially equal, there is a substantial discrepancy between the μFA , C_{MD} , and C_c values produced with QTI_{+} and QTI_{\pm} . Such discrepancy could play a major role when characterizing tissue heterogeneity via quantitative analysis. This would be especially relevant when analysing diseased tissues, such as brain tumors. The necrotic and oedematous tumor compartments typically contain large fractions of free water, which could bias the recovered

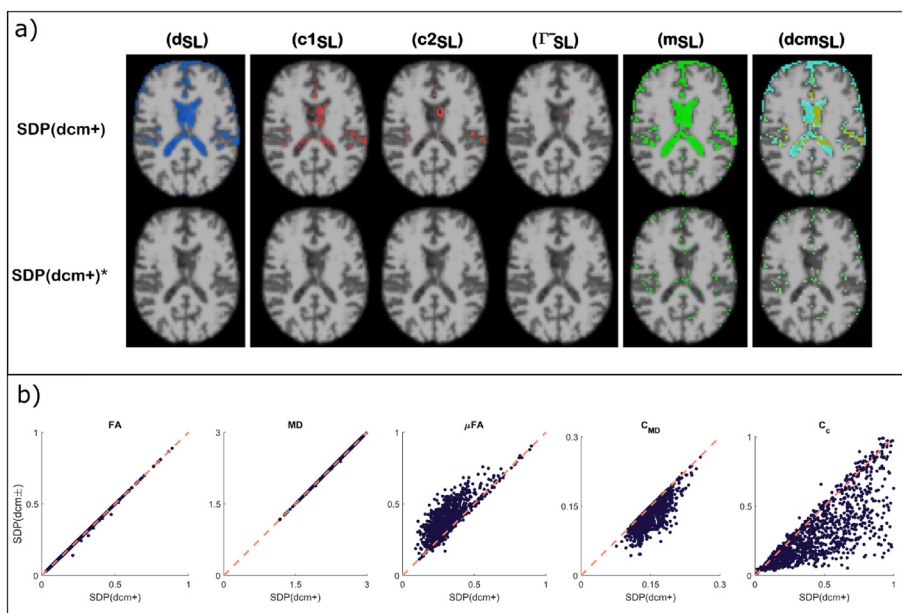


Fig. 5. a) Violations of the speed limit conditions for fits produced with SDP(dcm+) on the p81 dataset. The second row, marked with SDP(dcm+)*, shows the violations remaining after masking out the voxels in which the condition (d_{SL}) is not respected. Violations of condition (m_{SL}) can still be observed where partial voluming between different tissue types is occurring. The maximum allowed diffusivity was set to $D_0 = 3.0750 \mu\text{m}^2/\text{ms}$. b) Scatter plots comparing QTI stains computed from the fits produced employing QTI+ (SDP(dcm+)) and QTI± (SDP(dcm±)) on the voxels remaining after masking out those in which condition (d_{SL}) is not respected (a total of 1221 voxels across the all brain). The plots show that FA and MD have essentially equal values for the two fits, while μFA, C_{MD} and C_c may differ quite substantially.

metrics [20]. Therefore, methods accounting for possible artifacts arising from free water partial voluming should be considered for better *in vivo* assessment of tissue heterogeneity.

The results shown in Fig. 3 depicted the improvement introduced in the QTI stains when the diffusivity-limiting conditions are imposed. These results were consistent with those obtained on the datasets acquired during the study, thus demonstrating the validity of our findings across platforms. Note however that, as pointed out in section 3.2, some values of the constraint estimated μFA are pushed in the wrong direction. This is plausibly due to performing the fit on fewer data which are also already at the noise floor. Enforcing constraints under these conditions might produce biased estimates for parameters whose value is supposedly distributed around 0. As illustrated for example in Fig. 3 for the μFA values in the ventricles, this seems to manifest mostly on fits to datasets very sparsely sampled, such as p39 (results not shown) and p56. The effect is instead more contained on datasets comprising a higher number of data points, such as p217 (results not shown) and p81.

To be considered are also the run times reported in Table 1. The overall improvement in the parameters' estimation brought by performing constrained optimization comes at the cost of increasing the time it takes to estimate the model parameters. Future advances on the solvers' algorithmic side could help reduce the current processing time.

5. Conclusion

In this work we considered extending the list of conditions to be applied while fitting the QTI model, by adding constraints targeting the maximum allowed diffusivity. We showed that in regions where freely diffusing water is abundant these conditions are easily violated, with the violations plausibly due to contributions of different factors such as noise, CSF flow artifacts, and acquisition protocols not designed for data collection in these specific brain areas. Imposing the constraints helps the parameters derived from the QTI analysis to be directed towards their expected values, and generally provides stronger visual contrast between different brain tissues.

CRedit authorship contribution statement

Deneb Boito: Software, Validation, Investigation, Data curation, Writing – original draft, Writing – review & editing. **Magnus Herberthson:** Methodology, Formal analysis, Writing – original draft, Writing – review & editing. **Tom Dela Haije:** Methodology, Funding acquisition, Writing – review & editing. **Ida Blystad:** Supervision, Resources, Data curation, Writing – review & editing. **Evren Özarslan:** Conceptualization, Methodology, Formal analysis, Writing – review & editing, Supervision, Project administration, Funding acquisition, Writing – original draft.

Declaration of competing interest

EÖ and MH are shareholders in Spin Nord AB. The remaining authors declare no conflict of interest.

Acknowledgement

This research was funded by Sweden’s Innovation Agency (VINNOVA) ASSIST, Analytic Imaging Diagnostic Arena (AIDA), Swedish Foundation for Strategic Research (RMX18-0056), Linköping University Center for Industrial Information Technology (CENIIT), LiU Cancer Barncancerfonden, and a research grant (00028384) from VILLUM FONDEN.

Appendix. Derivation of the diffusivity-limiting conditions

In this appendix we discuss some of the inequalities presented in section 2.1.4.

Suppose that \mathbf{D}_{ij} is a stochastic variable which satisfies $0 \leq \mathbf{D}_{ij} \leq D_0 \mathbf{I}_{ij}$. For a non-zero vector u_j , which without loss of generalisation can be assumed to have unit length, from $M_{ijkl} = \langle D_{ij} D_{kl} \rangle$ it follows that $M_{ijkl} = \langle D_{ij} u_i u_j D_{kl} u_k u_l \rangle = \langle X^2 \rangle$, where $X = D_{ij} u_i u_j$, so that X takes values in $[0, D_0]$. This means that $\langle X^2 \rangle \leq D_0^2$, i.e., $M_{ijkl} u_i u_j u_k u_l \leq D_0^2 = D_0^2 I_{ij} I_{kl} u_i u_j u_k u_l$ which is condition (m_{SL}).

It can also be shown that the variance of the stochastic variable X satisfies $V(X) \leq D_0^2/4$. To see this, we first note that the variance is independent of translations, i.e., we can assume that X takes values in $[-d_0, d_0]$, where $d_0 = D_0/2$. The problem

can then be formulated as follows: suppose $\text{supp}(p) \subset [-d_0, d_0]$, $p \geq 0$, $\int_{-d_0}^{d_0} p(x) dx = 1$, $\int_{-d_0}^{d_0} xp(x) dx = \mu$. What is the maximal value of

$$\int_{-d_0}^{d_0} (x - \mu)^2 p(x) dx = \int_{-d_0}^{d_0} x^2 p(x) dx - \mu^2?$$

Let g be the even part of p , $g(x) = (p(x) + p(-x))/2$. Then $\int_{-d_0}^{d_0} xg(x) dx = 0$ and

$$\int_{-d_0}^{d_0} (x - 0)^2 g(x) dx = \int_{-d_0}^{d_0} x^2 \frac{p(x) + p(-x)}{2} dx = \int_{-d_0}^{d_0} x^2 p(x) dx \geq \int_{-d_0}^{d_0} x^2 p(x) dx - \mu^2 = \int_{-d_0}^{d_0} (x - \mu)^2 p(x) dx.$$

Hence, we can assume that p is even (so that $\mu = 0$). Next, since $p \geq 0$,

$$\int_{-d_0}^{d_0} x^2 p(x) dx \leq d_0^2 \int_{-d_0}^{d_0} p(x) dx = d_0^2 = D_0^2 / 4,$$

and this value is obtained for $p(x) = \frac{1}{2} \delta(x+d_0) + \frac{1}{2} \delta(x-d_0)$. Since $C_{ijkl} u_i u_j u_k u_l$ is precisely $V(x)$, (and since $I_{ij} u_i u_j = 1$), condition (Γ_{SL}^-) follows.

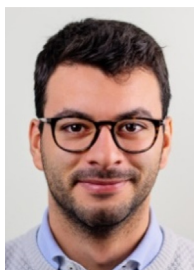
Conditions (c1_{SL}) and (c2_{SL}) can be proven by first considering that the coefficients $C_{\alpha\beta}$ are expressed with respect to an particular orthonormal set of basis matrices $\{A_1, A_2, A_3, A_4, A_5, A_6\}$ in the space of symmetric 3×3 matrices, with orthonormality taken with respect to the scalar product $\langle A, B \rangle = \text{tr}(AB)$. Namely, the three first matrices in the basis are $A_1 = \begin{pmatrix} 1 & 0 & 0 \\ 0 & 0 & 0 \\ 0 & 0 & 0 \end{pmatrix}$, $A_2 = \begin{pmatrix} 0 & 0 & 0 \\ 0 & 1 & 0 \\ 0 & 0 & 0 \end{pmatrix}$, $A_3 = \begin{pmatrix} 0 & 0 & 0 \\ 0 & 0 & 0 \\ 0 & 0 & 1 \end{pmatrix}$. Defining $X_1 = D_{ij}(A_1)_{ij}$, $X_2 = D_{ij}(A_2)_{ij}$, $X_3 = D_{ij}(A_3)_{ij}$, we get three stochastic variables taking values in $[0, D_0]$. Hence $0 \leq V(X_i) \leq D_0^2/4$, $i = 1, 2, 3$. For $1 \leq \alpha, \beta \leq 3$, $C_{\alpha\beta} = \text{Cov}(X_\alpha, X_\beta)$. Since $-\sqrt{V(X)V(Y)} \leq \text{Cov}(X, Y) \leq \sqrt{V(X)V(Y)}$, which results in condition (c1_{SL}).

Finally, note that if b_α is an eigenvector with eigenvalue λ to $C_{\alpha\beta}$, and if b_α has unit norm, then $C_{\alpha\beta} b_\alpha b_\beta = \lambda$. In terms of C_{ijkl} and the corresponding (eigen)matrix B_{ij} (with unit norm) this means that $C_{ijkl} B_{ij} B_{kl} = \lambda$. Define $Y = (D_{ij} - d_0 I_{ij}) B_{ij}$ with $d_0 = D_0/2$. Then $V(Y) = \langle (Y - \langle Y \rangle)(Y - \langle Y \rangle) \rangle = \langle ((D_{ij} - d_0 I_{ij}) B_{ij} - \langle (D_{ij} - d_0 I_{ij}) B_{ij} \rangle) ((D_{kl} - d_0 I_{kl}) B_{kl} - \langle (D_{kl} - d_0 I_{kl}) B_{kl} \rangle) \rangle = \langle (D_{ij} B_{ij} - \langle D_{ij} B_{ij} \rangle) (D_{kl} B_{kl} - \langle D_{kl} B_{kl} \rangle) \rangle = C_{ijkl} B_{ij} B_{kl}$. On the other hand,

$|Y| = |(D_{ij} - d_0 I_{ij}) B_{ij}| \leq \|(D_{ij} - d_0 I_{ij})\| \cdot \|B_{ij}\| = \|(D_{ij} - d_0 I_{ij})\|$. All the eigenvalues of $D_{ij} - d_0 I_{ij}$ lie in the range $[-d_0, d_0]$ and hence $\|(D_{ij} - d_0 I_{ij})\| \leq d_0 \|I_{ij}\| = \sqrt{3}d_0 = \sqrt{3}D_0/2$. By the earlier results, $V(Y) \leq 3D_0^2/4$, which proves condition (c2_{SL}).

References

- [1] C.F. Westin, H. Knutsson, O. Pasternak, F. Szczepankiewicz, E. Özarslan, D. van Westen, C. Mattisson, M. Bogren, L.J. O'Donnell, M. Kubicki, D. Topgaard, M. Nilsson, Q-space trajectory imaging for multidimensional diffusion MRI of the human brain, *Neuroimage* 135 (Jul 2016) 345–362.
- [2] T.M. de Swiet, P.P. Mitra, Possible systematic errors in single-shot measurements of the trace of the diffusion tensor, *J. Magn. Reson. B* 111 (Apr 1996) 15–22.
- [3] B. Jian, B.C. Vemuri, E. Özarslan, P.R. Carney, T.H. Mareci, A novel tensor distribution model for the diffusion-weighted MR signal, *Neuroimage* 37 (1) (2007) 164–176.
- [4] P.J. Basser, S. Pajevic, A normal distribution for tensor-valued random variables: applications to diffusion tensor MRI, *IEEE Trans. Med. Imag.* 22 (Jul 2003) 785–794.
- [5] E. Özarslan, N. Shemesh, C.G. Koay, Y. Cohen, P.J. Basser, Nuclear magnetic resonance characterization of general compartment size distributions, *New J. Phys.* 13 (2011), 15010.
- [6] M. Herberthson, D. Boito, T. Dela Haije, A. Feragen, C.-F. Westin, E. Özarslan, Q-space trajectory imaging with positivity constraints (QTI+), *Neuroimage* 238 (2021), 118198.
- [7] T. Dela Haije, E. Özarslan, A. Feragen, Enforcing necessary non-negativity constraints for common diffusion MRI models using sum of squares programming, *Neuroimage* 209 (2020), 116405.
- [8] D. Boito, M. Herberthson, T. Dela Haije, E. Özarslan, Enforcing positivity constraints in q-space trajectory imaging (QTI) allows for reduced scan time, in: *Proc Intl Soc Mag Reson Med*, vol. 29, 2021, 0404.
- [9] A. Ghosh, T. Milne, R. Deriche, Constrained diffusion kurtosis imaging using ternary quartics & MLE, *Magn. Reson. Med.* 71 (Apr. 2014) 1581–1591.
- [10] J. Veraart, W. Van Hecke, J. Sijbers, Constrained maximum likelihood estimation of the diffusion kurtosis tensor using a Rician noise model, *Magn. Reson. Med.* 66 (Sept. 2011) 678–686.
- [11] J. Mattiello, P.J. Basser, D. Le Bihan, The b matrix in diffusion tensor echo-planar imaging, *Magn. Reson. Med.* 37 (Feb 1997) 292–300.
- [12] D. Boito, M. Herberthson, T. Dela Haije, E. Özarslan, Applying positivity constraints to q-space trajectory imaging: the QTI+ implementation, *Software* 18 (2022), 101030.
- [13] K.C. Toh, M.J. Todd, R.H. Tütüncü, SDPT3 — a Matlab software package for semidefinite programming, version 1.3, *Optim. Methods Software* 11 (1–4) (1999) 545–581.
- [14] M. Grant, S. Boyd, CVX: Matlab Software for Disciplined Convex Programming, mar 2014 version 2.1, <http://cvxr.com/cvx>.
- [15] M. Grant, S. Boyd, Graph implementations for nonsmooth convex programs, in: V. Blondel, S. Boyd, H. Kimura (Eds.), *Recent Advances in Learning and Control*, Springer-Verlag Limited, 2008, pp. 95–110. *Lecture Notes in Control and Information Sciences*, http://stanford.edu/~boyd/graph_dcp.html.
- [16] F. Szczepankiewicz, S. Hoge, C.-F. Westin, Linear, planar and spherical tensor-valued diffusion MRI data by free waveform encoding in healthy brain, water, oil and liquid crystals, *Data Brief* 25 (Aug 2019) 104208.
- [17] M. Holz, S.R. Heil, A. Sacco, Temperature-dependent self-diffusion coefficients of water and six selected molecular liquids for calibration in accurate 1h nmr pfg measurements, *Phys. Chem. Chem. Phys.* 2 (2000) 4740–4742.
- [18] J.L. Andersson, S.N. Sotiropoulos, An integrated approach to correction for off-resonance effects and subject movement in diffusion MR imaging, *Neuroimage* 125 (Jan. 2016) 1063–1078.
- [19] J.-D. Tournier, R. Smith, D. Raffelt, R. Tabbara, T. Dhollander, M. Pietsch, D. Christiaens, B. Jeurissen, C.-H. Yeh, A. Connelly, MRtrix3: a fast, flexible and open software framework for medical image processing and visualisation, *Neuroimage* 202 (Nov. 2019) 116137.
- [20] L. Starck, F. Zaccagna, O. Pasternak, F.A. Gallagher, R. Grüner, F. Riemer, Effects of multi-shell free water correction on glioma characterization, *Diagnosics* 11 (12) (2021).



Deneb Boito received his B.S. degree in Biomedical Engineering from the University of Padua in 2015, and his M.Sc. degree in Biomedical Engineering from Linköping University in 2018. He is currently a Doctoral Student at Linköping University under the supervision of Dr. Evren Özarslan. He specializes in diffusion magnetic resonance imaging methods and data processing for characterizing the microstructure of the human brain.



Evren Özarslan received his bachelor's degree in Physics from the University of Illinois, Urbana-Champaign and his PhD from University of Florida where he also obtained a master's degree in Biomedical Engineering. He worked in Peter J. Basser's lab at the National Institutes of Health, first as a postdoctoral fellow, then as a scientist with the Center for Neuroscience and Regenerative Medicine. Evren subsequently accepted a position with the Department of Radiology, Brigham and Women's Hospital, where he was promoted to the rank of assistant professor at Harvard Medical School. In 2013, Evren moved to Istanbul where he was an assistant professor in the Department of Physics at Boğaziçi University. Since early 2016, he has been with the Department of Biomedical Engineering, Linköping University in Sweden. Evren's current research is on developing innovative magnetic resonance techniques with the aim of characterizing water dynamics within biological tissues as well as other porous media.